WRNIP1 PREVENTS TRANSCRIPTION-ASSOCIATED GENOMIC INSTABILITY

Pasquale Valenzisi[1#], Veronica Marabitti[1#], Pietro Pichierri[1] and Annapaola Franchitto[1*]

Section of Mechanisms Biomarkers and Models, Department of Environment and Health, Istituto Superiore di Sanita', Viale Regina Elena 299, Rome, 00161, Italy.

[#] These two authors contributed equally to this work

[*] To whom correspondence should be addressed. Tel: +39 0649903042; Fax: +39 0649903650.

Email: annapaola.franchitto@iss.it

Keywords: Genomic instability, Replication stress, R-loops, Werner helicase-interacting protein 1.

ABSTRACT

R-loops are non-canonical DNA structures that form during transcription and play diverse roles in various physiological processes. Disruption of R-loop homeostasis can lead to genomic instability and replication impairment, contributing to several human diseases, including cancer. Although the molecular mechanisms that protect cells against such events are not fully understood, recent research has identified the fork protection factors and the DNA damage response proteins as regulators of R-loop dynamics. Here, we identify the Werner helicase-interacting protein 1 (WRNIP1) as a novel factor that counteracts transcription-associated DNA damage upon replication perturbation. Loss of WRNIP1 leads to R-loop accumulation, resulting in collisions between the replisome and transcription machinery. We observe co-localization of WRNIP1 with transcription/replication complexes and R-loops after replication perturbation, suggesting its involvement in resolving transcription-replication conflicts. Moreover, WRNIP1-deficient cells show impaired replication restart from transcription-induced fork stalling. Notably, transcription inhibition and RNase H1 overexpression rescue all the defects caused by loss of WRNIP1. Importantly, our findings highlight the critical role of WRNIP1 ubiquitin-binding zinc finger (UBZ) domain in preventing pathological persistence of R-loops and limiting DNA damage, thereby safeguarding genome integrity.

INTRODUCTION

Maintenance of genome integrity is essential for cell viability and relies on complete and accurate DNA replication. However, genome is continuously threatened by several types of DNA lesions that hinder replication fork progression, leading to fork stalling and replication stress and ultimately to genomic instability, a hallmark of cancer cells. Different molecular mechanisms underlie replication stress in cells, and understanding how they occur has always been of interest for targeting them for cancer therapy. Among known mechanisms that perturb genome duplication, the transcription process plays a crucial role in inducing stalling of replication forks. Indeed, transcription can not only hamper replication fork progression itself but can also act as an enhancer of replication impediments, such as protein-DNA complexes, DNA damage and non-B-form DNA secondary structures (Gómez-González and Aguilera 2019). Among the latter, R-loops have emerged as critical determinants of transcription-associated replication stress. R-loops can cause genomic instability and may promote cancer and other human diseases (Gómez-González and Aguilera 2019; García-Muse and Aguilera 2019; Crossley and Cimprich 2019). R-loops are three-stranded structures that consist of an DNA/RNA hybrid and a displaced single-stranded DNA. They are involved in various physiological processes, including transcription termination, regulation of gene expression, and DNA repair. Under physiological conditions, R-loops are transient structures that are resolved by enzymes (Sanz et al. 2016; Wahba et al. 2011). However, if they persist, they can become pathological and provoke the formation of transcription-replication conflicts (TRCs). Given the high frequency at which replication and transcription processes occur in cells, TRCs are particularly likely to happen. Additionally, the interference between transcription and replication at very large human genes, whose transcription continues into S-phase, may contribute to the instability of common fragile sites (CFS), the most replication stress-sensitive regions in the human genome (Helmrich and Tora 2011). Notably, the idea that R-loops cause fork stalling, promoting TRCs and leading to transcription-associated DNA damage, is supported by the fact that many strategies aimed at minimizing collisions and facilitating replication fork progression following unscheduled R-loop accumulation rely on replication fork protection factors and DNA damage response (DDR) proteins (Shivji et al. 2018; Hatchi et al. 2015; Schwab et al. 2015; García-Rubio et al. 2015; Bhatia et al. 2014; Liang et al. 2019; Urban et al. 2016; Chang et al. 2017; Marabitti et al. 2019; Tresini et al. 2015) . The precise mechanisms by which cells cope with TRCs resulting from persistent R-loops are still largely unknown.

Human WRN-interacting protein 1 (WRNIP1) is a genome maintenance factor (Yoshimura and Enomoto 2017). WRNIP1 binds to forked DNA that resembles stalled forks (Yoshimura et al. 2009) and its foci overlap with replication factories (Crosetto et al. 2008), suggesting a role at replication forks. Consistent with this, WRNIP1 protects stalled forks from MRE11-mediated degradation and promotes fork restart upon replication stress (Leuzzi et al. 2016; Porebski et al. 2019). Alongside its

role at forks, WRNIP1 is implicated in ATM-dependent checkpoint activation in response to mild replication stress (Kanu et al. 2016; Marabitti et al. 2020). Notably, in cells with defective ATR-dependent checkpoint activation, such as Werner syndrome cells (Basile et al. 2014), WRNIP1 mediates ATM-dependent CHK1 phosphorylation to counteract pathological R-loop accumulation (Marabitti et al. 2020). In addition, WRNIP1 is found to be enriched at CFS, suggesting a role in maintaining their stability (Pladevall-Morera et al. 2019). However, data concerning a role of WRNIP1 in restricting transcription-associated genomic instability are not available.

Here, we uncover that loss of WRNIP1 and the activity of WRNIP1 ubiquitin-binding zinc finger (UBZ) domain are required for limiting unscheduled R-loops that give rise to TRCs. Furthermore, we establish that loss of WRNIP1 functions is accountable for the increased genomic instability observed in WRNIP1-deficient and WRNIP1 UBZ mutant cells upon mild replication perturbation.

RESULTS

Transcription-dependent DNA damage occurs in WRNIP1-deficient and WRNIP1 UBZ mutant cells upon MRS

To investigate the contribution of WRNIP1 in maintaining genome integrity, we evaluated DNA damage accumulation in response to mild replication stress (MRS) induced by nanomolar dose of the DNA polymerase inhibitor aphidicolin (Aph). In addition to its ATPase activity, which is involved in fork restart (Leuzzi et al. 2016), WRNIP1 also contains an ubiquitin-binding zinc finger (UBZ) domain. Although this domain has been implicated in fork-related functions (Yoshimura et al., 2017), its function is still poorly defined.

In our experiments, we used the SV40-transformed MRC5 fibroblast cell line (MRC5SV), MRC5SV cells stably expressing WRNIP1-targeting shRNA (shWRNIP1) and isogenic cell lines stably expressing the RNAi-resistant full-length wild-type WRNIP1 (shWRNIP1^{WT}), its ATPase-dead mutant form (shWRNIP1^{T294A}) (Leuzzi et al. 2016) or the UBZ-dead mutant form of WRNIP1 (shWRNIP1^{D37A}) that abolishes the ubiquitin-binding activity (Bish and Myers 2007; Nomura et al. 2012) (Figure 1A). Initially, we measured DNA damage by a single-cell electrophoresis in WRNIP1-deficient and WRNIP1 mutant cells. In agreement with previous experiments (Marabitti et al. 2020), we found that loss of WRNIP1 resulted in higher spontaneous levels of DNA damage compared to wild-type cells (MRC5SV), and that Aph exacerbated this phenotype (Figure 1B). Interestingly, in WRNIP1 mutant cells, spontaneous genomic damage was similar to that observed in WRNIP1-deficient cells but, after MRS, it was significantly enhanced only in WRNIP1 UBZ mutant cells (Figure 1B).

137 In parallel experiments, we assessed the presence of chromosomal damage. As shown in Figure 1C,
138 shWRNIP1 and WRNIP1 mutant cells exhibited a greater number of chromosomal aberrations under
139 unperturbed conditions, compared to their corrected isogenic counterparts (shWRNIP1^{WT}). However,
140 while loss of WRNIP1 or mutation of its UBZ domain heightened the average number of gaps and
141 breaks after Aph than their corrected counterparts (shWRNIP1^{WT}), that of ATPase activity did not
142 (Figure 1C). Therefore, loss of WRNIP1 or its ubiquitin-binding function renders cells highly
143 sensitive to Aph-induced MRS, affecting genomic integrity.
144 We next wondered whether DNA damage accumulated in a transcription-dependent manner. To test
145 this possibility, we performed a Comet assay using MRC5SV, shWRNIP1, shWRNIP1^{D37A} and
146 shWRNIP1^{T294A} cells incubated with Aph and/or the 5,6-dichloro-1-ß-D-ribofurosylbenzimidazole
147 (DRB), a strong inhibitor of RNA synthesis, as described (Marabitti et al. 2019). Our analysis showed
148 that DNA damage was not sensitive to transcription inhibition at any of the tested conditions in wild-
149 type and WRNIP1 ATPase mutant cells (Figure 1D). In contrast, DRB significantly suppressed the
150 amount of DNA damage in both shWRNIP1 and shWRNIP1^{D37A} cells that were either untreated or
151 treated with Aph (Figure 1D). Similar results were obtained using another transcription inhibitor,
152 Cordycepin (3'-deoxyadenosine) ((Müller et al. 1977); Suppl Figure 1A). Additionally, anti-phospho-
153 H2AX immunostaining, which is considered an early sign of DNA damage caused by replication fork
154 stalling (Ward and Chen 2001), confirmed a transcription-dependent DNA damage accumulation in
155 shWRNIP1 and shWRNIP1^{D37A} cells (Suppl Figure 1B).
156 Altogether these findings suggest that WRNIP1 and the activity of its UBZ domain are required to
157 prevent transcription-dependent DNA damage.
158
159 **Enhanced R-loop accumulation is observed in WRNIP1-deficient cells**
160 The main structures associated with transcription that can impede fork movement and result in
161 transcription-replication conflicts (TRCs) are R-loops (Gan et al. 2011; Allison and Wang 2019;
162 Gaillard and Aguilera 2016). As WRNIP1 may counteract R-loop-mediated TRCs by reducing
163 transcription-dependent DNA damage accumulation, we first assessed R-loops levels in our cells
164 using the well-established anti-RNA-DNA hybrid S9.6 antibody (Boguslawski et al. 1986; Hamperl
165 et al. 2017; Marabitti et al. 2019). We observed a significant increase in nuclear S9.6 intensity in
166 unperturbed WRNIP1-deficient cells, but not in their corrected counterparts (shWRNIP1^{WT}; Figure
167 2A). Furthermore, while Aph treatment caused increased R-loop levels in both cell lines, the values
168 were considerably higher in shWRNIP1 cells (Figure 2A). Importantly, the S9.6 staining was strongly
169 suppressed upon overexpression of RNaseH1 that removes R-loops (Cerritelli et al. 2003) (Figure
170 2A).

171 To further confirm the accumulation of R-loop within nuclear DNA, we isolated genomic DNA from
172 shWRNIP1^{WT} and shWRNIP1 cells and performed a dot blot analysis. Consistent with fluorescence
173 analysis, the S9.6 signal was higher in shWRNIP1 cells than in shWRNIP1^{WT} cells and was abolished
174 by RNaseH treatment (Figure 2B; (Morales et al. 2016)). This result suggest that DNA damage
175 observed in WRNIP1-deficient cells may be correlated with the elevated accumulation of R-loops.
176
177 **Loss of WRNIP1 or its UBZ domain results in R-loop-dependent DNA damage upon MRS**
178 After demonstrating that WRNIP1-deficient cells accumulate high levels of R-loops, we investigated
179 the risks to genome integrity by comparing different replication stress conditions. As observed above,
180 loss of WRNIP1 slightly increased the amount of spontaneous DNA damage, while Aph enhanced
181 the comet tail moment to a greater extent in shWRNIP1 than in MRC5SV cells (Figure 3A). A similar
182 trend was observed using hydroxyurea (HU) as a replication-perturbing agent (Figure 3A). It is
183 noteworthy that overexpression of RNaseH1 was able to strongly reduce the tail moment only in
184 shWRNIP1 cells and more efficiently after Aph-induced replication slowdown than arrest by HU
185 (Figure 3A). This confirms R-loops as a driver of genome instability in WRNIP1-deficient cells and
186 suggests that R-loop-mediated DNA damage is more pronunced after a replication stress that does
187 not completely block replication fork progression.
188 Next, we asked which of the WRNIP1 activities could prevent the formation of aberrant R-loops upon
189 MRS. We observed a similar level of spontaneous R-loops in cells with mutations in either ATPase
190 or UBZ domain. However, following MRS, shWRNIP1^{D37A} cells exhibited a more pronounced S9.6
191 signal than shWRNIP1^{T294A} cells (Figure 3B), indicating a role for the UBZ domain of WRNIP1 in
192 counteracting R-loop accumulation upon MRS.
193 Finally, we wanted to determine whether R-loop-mediated DNA damage in WRNIP1-deficient cells
194 was due to the loss of the UBZ domain of WRNIP1. Notably, we found that suppression of DNA
195 damage in shWRNIP1^{D37A} cells upon RNaseH1 overexpression was similar to that seen in shWRNIP1
196 cells (Figure 3C), suggesting that the ubiquitin-binding activity of WRNIP1 is necessary to prevent
197 R-loop-mediated DNA damage upon MRS.
198
199
200
201 **The UBZ domain of WRNIP1 is required to attenuate TRCs upon MRS**
202 Since TRCs play a crucial role in promoting R-loop-mediated genomic instability (García-Muse and
203 Aguilera 2016), we investigated the occurrence of such conflicts under our conditions. Hence, we
204 performed a proximity ligation assay (PLA), a well-established method for detecting physical

interactions (Söderberg et al. 2008). In this assay we utilized antibodies against proliferating cell nuclear antigen (PCNA) and RNA polymerase II (RNA pol II) to label replication forks and transcription complexes, respectively, as previously described (Hamperl et al. 2017). Our analysis revealed a higher number of spontaneous PLA signals (indicated by red spots) in WRNIP1-deficient and WRNIP1 UBZ mutant cells compared to wild-type cells (Figure 4A). Importantly, although Aph increased the co-localization of PCNA and RNA pol II in all cell lines, the number of PLA spots was significantly greater in shWRNIP1 and shWRNIP1^{D37A} cells than in shWRNIP1^{WT} cells (Figure 4A). Interestingly, this phenotype was substantially reduced by overexpressing RNaseH1 (Figure 4A), suggesting that the UBZ domain of WRNIP1 may play a role in attenuating R-loop-induced TRCs upon MRS.

Next, we examined the localization of WRNIP1 near/at transcription and replication machineries by conducting PLA assays in shWRNIP1^{WT} and shWRNIP1^{D37A} cells. For this purpose, we used antibodies against WRNIP1 and RNA pol II or PCNA, respectively. Our findings support the notion that WRNIP1 is indeed localized at the sites of TRCs following treatment with Aph in wild-type cells, as evidenced by an increased number of PLA spots between WRNIP1 and RNA pol II (Figure 4B), as well as between WRNIP1 and PCNA (Figure 4C). Surprisingly, a similar, but more pronounced, phenotype was observed in WRNIP1 UBZ mutant cells compared to wild-type cells, both under normal conditions and after treatment (Figures 4B and C).

Furthermore, we explored the localization of WRNIP1 in proximity to R-loops. Through the PLA assay we noticed a growing number of spots, indicating the presence of interactions between WRNIP1 and R-loops (anti-S9.6) (Figure 4D). Interestingly, this phenomenon was more evident in WRNIP1 UBZ mutant cells (Figure 4D), suggesting that WRNIP1, along with its UBZ domain, plays a role in the response to R-loop accumulation.

One of the initial steps in resolving R-loops involves the recruitment of RAD51 to stalled forks (Chappidi et al. 2020). Our PLA assay revealed that RAD51-R-loops nuclear spots were clearly observed in both MRC5SV and shWRNIP1^{D37A} cell lines following Aph treatment, but their presence was reduced in WRNIP1 UBZ mutant cells compared to wild-type cells (Figure 4E).

Taken together, these findings suggest that WRNIP1 co-localizes with transcription/replication complexes and R-loops following MRS. Additionally, they indicate that the ubiquitin-binding function of WRNIP1 helps to mitigate R-loop-mediated TRCs.

Transcription-mediated R-loop formation can act as a barrier to DNA replication in cells lacking WRNIP1 or its UBZ domain activity

R-loops are transcription-associated structures that can impede the progression of replication forks (Belotserkovskii et al. 2018). To assess the direct impact of R-loops on fork progression, we

239 performed a DNA fiber assay to examine replication fork dynamics at the single molecule level in
240 Aph-treated MRC5SV, shWRNIP1 and WRNIP1 UBZ mutant cells. Cells were labelled sequentially
241 with the thymidine analogues 5-chloro-2'-deoxyuridine (CldU) and 5-iodo-2'-deoxyuridine (IdU), as
242 described in the scheme (Figure 5A). Under normal growth conditions, and in agreement with
243 previous data (Leuzzi et al. 2016), MRC5SV and shWRNIP1 cells exhibited nearly identical fork
244 velocities, while shWRNIP1^{D37A} cells showed a significantly reduced velocity (Figure 5A). Following
245 Aph treatment, fork velocity decreased in all cell lines, but values were markedly lower in cells
246 lacking WRNIP1 or its UBZ domain (Figure 5B). Importantly, RNaseH1 overexpression led to a
247 significant increase in the rate of fork progression only in shWRNIP1 and shWRNIP1^{D37A} cells
248 (Figure 5A and B). DNA fiber analysis also revealed that loss of WRNIP1 or its UBZ domain resulted
249 in a greater percentage of stalled forks induced by Aph compared to control cells (Figure 5C).
250 Moreover, when comparing the percentage of restarting forks in all cell lines, we observed that the
251 absence of WRNIP1 reduced the ability of cells to resume replication after release from Aph to the
252 same extent as the loss of its UBZ domain (Figure 5D). Suppressing R-loop formation lowered the
253 percentage of stalled forks and, consistently, increased that of restarting forks in both shWRNIP1 and
254 shWRNIP1^{D37A} cells (Figure 5 C and D). Similar results were obtained by treating cells with DRB
255 (Suppl. Figure 2A-D).
256 Therefore, we concluded that in cells lacking WRNIP1 or its UBZ domain, R-loops can pose a
257 significant impediment to replication. Additionally, the ubiquitin-binding activity of WRNIP1 may
258 play a crucial role in restarting replication when transcription-induced fork stalling occurs.
259
260 **FA pathway is correctly activated in WRNIP1-deficient or WRNIP1 UBZ mutant cells**
261 Previous studies have demonstrated that a functional Fanconi anaemia (FA) pathway prevents the
262 unscheduled accumulation of transcription-associated R-loops, with FANCD2 monoubiquitination
263 playing a critical role (Liang et al. 2019). Additionally, it has been reported that the FANCD2 protein
264 complex contains WRNIP1, which, under certain conditions, facilitates the binding of the
265 monoubiquitinated FANCD2/FANCI complex to DNA through its UBZ domain (Socha et al. 2020).
266 Hence, to gain insight into defective R-loop resolution, we assessed the functional status of the FA
267 pathway in our cells by examining FANCD2 monoubiquitination, a well-established readout of FA
268 pathway activation (Taniguchi et al. 2002). To this end, we treated MRC5SV, shWRNIP1 and
269 shWRNIP1^{D37A} cells with Aph and/or DRB and performed Western blotting analysis (Figure 6A).
270 Our results showed that loss of WRNIP1 or its UBZ domain did not affect FANCD2 ubiquitination
271 after treatments, indicating that the FA pathway was properly activated under our conditions (Figure
272 6A). Consistently, we observed comparable FANCD2 relocalization during R-loop-associated

replication stress in all cell lines tested, and it was reduced by transcription inhibition, providing further evidence of proper FA pathway activation (Suppl. Figure 3A). In agreement with previous findings (Wells et al. 2022), we found that RAD18 plays a role in FANCD2 recruitment upon MRS (Suppl. Figure 3B). Moreover, PLA assay demonstrated that, under our conditions, FANCD2 was localized near/at R-loops (anti S9.6) after Aph with a greater number of spots in shWRNIP1^{D37A} cells compared to control cells (Figure 6B).

We then conducted a Comet assay in MRC5SV, shWRNIP1 and shWRNIP1^{D37A} cells depleted of FANCD2 to investigate the potential association between WRNIP1 and the FANCD2 pathway under replication stress. Our results revealed increased spontaneous DNA damage in both the shWRNIP1 and shWRNIP1^{D37A} cells in which FANCD2 has been depleted (Figure 6C). Interestingly, disruption of FANCD2 led to a higher degree of DNA damage upon replication stress induced by Aph in the shWRNIP1 and shWRNIP1^{D37A} cells compared to control cells (Figure 6C).

These findings collectively suggest that FANCD2 and WRNIP1 may not be inherently interconnected.

DISCUSSION

Discovered as one of the interactors of the WRN helicase (Kawabe et al. 2001; Kawabe et al. 2006), the precise function of WRNIP1 in human cells is largely unknown. Previous results from our lab and others have revealed that WRNIP1 is crucial for the protection of HU-stalled replication forks (Leuzzi et al. 2016; Porebski et al. 2019). More recently, it has been shown that checkpoint defects elicit a WRNIP1-mediated response to limit R-loop-associated genomic instability (Marabitti et al. 2020). However, it remains unclear whether WRNIP1 is directly involved in the mechanisms of R-loop removal/resolution. In this study, we establish a function for WRNIP1 and its ubiquitin-binding zinc finger (UBZ) domain in counteracting DNA damage and genome instability resulting from transcription-replication conflicts (TRCs).

We have demonstrated that WRNIP1 contributes to fork restart, and that this function requires its ATPase activity (Leuzzi et al. 2016). It is noteworthy that although the ATPase activity of WRNIP1 is important for the restart of stalled forks (Leuzzi et al. 2016), it is dispensable to cope with TRCs. In sharp contrast, a mutation that disrupts the WRNIP1 UBZ domain (Bish and Myers 2007; Nomura et al. 2012) is sufficient to stimulate TRCs and DNA damage at levels comparable to, if not higher than, those detected in WRNIP1-deficient cells. The persistence of R-loops is deleterious because they may interfere with DNA replication, and R-loop-mediated fork stalling is a major feature of TRCs (Gan et al. 2011; Boubakri et al. 2010; Wellinger et al., 2006; Tuduri et al. 2009). In WRNIP1-deficient or WRNIP1 UBZ mutant cells, the elevated DNA damage and reduced fork speed are

307 reverted by RNase H1-GFP overexpression, which degrades RNA/DNA hybrids and wipes out R-
308 loops (Cerritelli et al. 2003). In line with this, many more R-loops are detected in WRNIP1-deficient
309 or WRNIP1 UBZ mutant cells. This suggests that unscheduled R-loops are likely responsible for the
310 increased levels of TRCs, the marked replication defects, and genomic instability observed in the
311 absence of WRNIP1.
312 R-loops are the main DNA secondary structures formed during transcription and, although they
313 regulate several physiological processes, they can also act as potent replication fork barriers (Crossley
314 et al., 2019; Gómez-González and Aguilera 2019). Consequently, the unscheduled accumulation of
315 R-loops leads to TRCs, creating transcription-associated DNA damage in both yeast and human cells
316 (Huertas and Aguilera 2003; Li and Manley 2005; Santos-Pereira and Aguilera 2015; Sollier et al.
317 2014; Paulsen et al. 2009). To prevent TRCs, several replication fork protection factors are essential
318 (Chang and Stirling 2017). Disrupting any of these proteins can affect the ability of cells to overcome
319 or resolve R-loops, leading to DNA damage.
320 Our previous research has established that WRNIP1, although not through its ATPase activity, can
321 protect stalled forks from nucleolytic degradation upon replication stress (Leuzzi et al. 2016). In
322 addition, WRNIP1 has been shown to immunoprecipitate with BRCA2 and RAD51, and loss of
323 WRNIP1 has been found to destabilize RAD51 on ssDNA (Leuzzi et al. 2016) Notably, when R-loop
324 is formed, it can expose a potentially vulnerable single-stranded DNA (ssDNA) region on the non-
325 template strand (Aguilera and García-Muse 2012). Since BRCA2 is kwon to play an important role
326 in mitigating R-loop-induced DNA damage (Shivji et al. 2018; Bhatia et al. 2014; Wang et al. 2022),
327 it is possible that WRNIP1, through its association with the BRCA2/RAD51 complex, could promote
328 RAD51 recruitment or stabilization to protect the ssDNA of R-loops. In support of this, RAD51 co-
329 localizes with R-loops after MRS and this co-localization is dependent on the WRNIP1 UBZ domain.
330 Therefore, WRNIP1 may protect R-loops to ensure their safe handling and promote the successful
331 restart of stalled forks. Consistent with this hypothesis, we observe WRNIP1 co-localizing with
332 transcription/replication complexes and R-loops after MRS. It has been proposed that R-loop incision,
333 which promotes fork progression and restart at TRCs (Chappidi et al. 2020), requires high accuracy
334 to avoid fork collapse and chromosomal damage, putting genome integrity at risk (Sollier et al. 2014;
335 Promonet et al. 2020). Our findings show that R-loop-dependent accumulation of DNA damage and
336 genome instability, which may indicate preferential engagement of error-prone mechanisms upon
337 WRNIP1 depletion. Alternatively, WRNIP1 may stabilize RAD51 on the ssDNA of DNA/RNA
338 hybrids and promote fork restart through fork reversal. Indeed, one proposed mechanism for
339 processing DNA/RNA hybrids involves exposing ssDNA and loading RAD51, which mediates fork
340 reversal (Stoy et al. 2023). While these hybrids are resolved under physiological conditions, allowing

341 stalled fork restart (Stoy et al. 2023; Chappidi et al. 2020), post-replicative DNA/RNA hybrids would
342 represent pathological TRC intermediates that can impair replication fork progression and stimulate
343 fork reversal.
344 The phenotype of WRNIP1 UBZ mutant cells and WRNIP1-depleted cells is similar, suggesting that
345 the ubiquitin-binding function of WRNIP1 could help mitigate R-loop-induced TRCs. Although the
346 UBZ domain of WRNIP1 still has an undefined function after replication perturbation (Yoshimura et
347 al., 2017), human WRNIP1 binds to both forked DNA, which resembles stalled replication forks, and
348 to template/primer DNA in an ATP-dependent fashion (Yoshimura et al. 2009). However, our
349 findings suggest that WRNIP1 does not use its ATPase activity to counteract TRC-induced R-loops
350 accumulation. Nevertheless, WRNIP1's ability to bind ubiquitin indicates that it may be implicated
351 in the metabolic processes of ubiquitinated proteins (Bish and Myers 2007). The UBZ domain of
352 WRNIP1 is involved in the physical association with RAD18 (Kanu et al. 2016) RAD18-deficient
353 cells exhibit high levels of TRCs and accumulate DNA/RNA hybrids, which induce DNA double
354 strand breaks and replication stress (Wells et al. 2022). These effects are, in part, dependent on the
355 inability to recruit the Fanconi anaemia protein FANCD2 to R-loop prone genomic sites (Wells et al.
356 2022). Notably, in our context, FANCD2 localizes with R-loops after MRS, and this localization is
357 more pronounced in cells lacking the WRNIP1 UBZ domain. Additionally, in our cell lines, FA
358 pathway may serve as a backup system to counteract TRCs. Therefore, it is tempting to speculate that
359 the UBZ domain might contribute to direct WRNIP1 to DNA at TRC sites through RAD18 and that
360 the elevated levels of TRCs observed in RAD18-deficient cells are due to the loss of both WRNIP1
361 and FANCD2 functions. This interesting point deserves further and detailed investigation.
362 Altogether our findings reveal a previously unappreciated role for WRNIP1 in counteracting the
363 pathological accumulation of transcription-associated R-loops, which ultimately leads to heightened
364 genomic instability following MRS in human cells. A growing body of evidence suggests that R-
365 loops may underlie the genomic instability observed in human cancer cells (Crossley et al., 2019;
366 García-Muse and Aguilera 2019) Moreover, given that WRNIP1 is found to be overexpressed in the
367 most common human cancer types, such as lung and breast cancers, our discoveries expand our
368 comprehension of the mechanisms employed by cells to avert TRCs. These results pave the way for
369 exploring novel pathways that contribute to genomic instability in cancer.

370 **MATERIALS AND METHODS**

371

372 **Cell lines and culture conditions**

373 The SV40-transformed MRC5 fibroblast cell line (MRC5SV) was a generous gift from Patricia
374 Kannouche (IGR, Villejuif, France). MRC5SV cells stably expressing WRNIP1-targeting shRNA
375 (shWRNIP1) and isogenic cell lines stably expressing the RNAi-resistant full-length wild-type
376 WRNIP1 (shWRNIP1^{WT}), its ATPase-dead mutant form (shWRNIP1^{T294A}) were generated as
377 previous reported (Leuzzi et al. 2016). By using the Neon^{TM} Transfection System Kit (Invitrogen)
378 according to the manufacturer's instructions, shWRNIP1 cells were stably transfected with a plasmid
379 expressing a FLAG-tagged full-length WRNIP1 plasmid carrying Ala substitution at Asp37 site
380 missense-mutant form of WRNIP1 with dead form of ubiquitin-binding zinc finger (UBZ) domain
381 (WRNIP1^{D37A}) (Yoshimura et al., 2017), Cells were cultured in the presence of neomycin and
382 puromycin (1 mg/ml and 100 ng/ml, respectively) to maintain selective pressure for expression.
383 All cell lines were maintained in DMEM media supplemented with 10% FBS, 100 U/mL penicillin
384 and 100 mg/mL streptomycin and incubated at 37°C in an humified 5% CO_2 atmosphere.

385

386 **Site-directed mutagenesis and cloning**

387 Site-directed mutagenesis of the WRNIP1 full-lenght cDNA (Open Biosystems) was performed on
388 the pCMV-FLAGWRNIP1 plasmid that contains the wild-type ORF sequence of WRNIP1.
389 Substitution of Asp37 to Ala in pCMV-FLAGWRNIP1 was introduced by the Quick-change XL kit
390 (Stratagene) using mutagenic primer pairs designed, according to the manufacturer's instructions.
391 Each mutated plasmid was verified by full sequencing of the WRNIP1 ORF.

392

393 **Chemicals**

394 Chemicals used were commercially obtained for the replication stress-inducing drug: aphidicolin
395 (Aph, Sigma-Aldrich), hydroxyurea (HU, Sigma-Aldrich) and the transcription elongation inhibitor
396 5,6-dichloro-1-ß-D-ribofurosylbenzimidazole (DRB, Sigma-Aldrich). The final concentrations of the
397 drugs used were: 0.4 aphidicolin, 4 mM HU and 50 μM DRB. Stock solutions for all the chemicals
398 were prepared in DMSO at a concentration of >1000. The final concentration of DMSO in the culture
399 medium was always < 0.1%.

400

401 **Plasmids and RNA interference**

402 The construct used to perform RNaseH1 overexpression experiments is a generous gift from Prof.
403 R.J. Crouch (National Institutes of Health, Bethesda, USA). As previously described (Cerritelli et al.

404 2003), the GFP-tagged RNaseH1 plasmid was generated by introducing a mutation on Met27
405 abrogating mitochondrial localization signal (RNaseH1-M27). To express the plasmids, cells were
406 transfected using the Neon™ Transfection System Kit (Invitrogen), according to the manufacturer's
407 instructions.
408 FANCD2 genetic knockdown experiment was performed by Interferin (Polyplus), according to the
409 manufacturer's instructions with Silencer Select siRNA (Thermo Fischer) targeting the following
410 region of the mRNA (5'-CAGCCUACCUGAGAUCCUAtt-3'). siRNA was used at 2.5 nM. As a
411 control, a siRNA duplex directed against GFP was used. Depletion was confirmed by Western blot
412 using the relevant antibodies (*see below*).
413
414 **Western blot analysis**
415 The proteins were resolved on polyacrylamide gels and transferred onto nitrocellulose membrane
416 using the Trans-Blot Turbo Transfer System (Bio-Rad). The membranes were blocked using 5%
417 NFDM in TBST (50 mM Tris/HCl pH 8, 150 mM NaCl, 0.1% Tween-20), and incubated with
418 primary antibody for 1 h at RT. The primary antibodies used for WB were: rabbit-polyclonal anti-
419 WRNIP1 (Bethyl Laboratories, 1:2500), mouse-monoclonal anti-FLAG (Sigma-Aldrich, 1:1000),
420 mouse-polyclonal anti-GAPDH (Millipore, 1:5000), mouse-monoclonal anti-FANCD2 (Santacruz;
421 1:500) and rabbit-polyclonal anti-LAMIN B1 (Abcam, 1:30000).
422 The membranes were incubated with horseradish peroxidase-conjugated goat specie-specific
423 secondary antibodies (Santa Cruz Biotechnology, 1:20000), for 1 h at RT. Visualisation of the signal
424 was accomplished using Western Bright ECL HRP substrate (Advansta) and imaged using Chemidoc
425 XSR+ (Chemidoc Imaging Systems, Bio-Rad).
426
427 **Chromosomal aberrations**
428 Cells for metaphase preparations were collected according to standard procedure and as previously
429 reported (Pirzio et al. 2008). Cell suspension was dropped onto cold, wet slides to make chromosome
430 preparations. The slides were air dried overnight, then for each condition of treatment, the number of
431 breaks and gaps was observed on Giemsa-stained metaphases. For each time point, at least 50
432 chromosome metaphases were examined by two independent investigators, and chromosomal
433 damage was scored at 100× magnification with an Olympus fluorescence microscope.
434
435 **Alkaline Comet assay**
436 DNA breakage induction was examined by alkaline Comet assay (single-cell gel electrophoresis) in
437 denaturing conditions as described (Pichierri et al. 2001). Cell DNA was stained with a fluorescent

438 dye GelRed (Biotium) and examined at 40× magnification with an Olympus fluorescence microscope
439 and examined at 40× magnification with an Olympus fluorescence microscope. Slides were analysed
440 by a computerized image analysis system (CometScore, Tritek Corp). To assess the amount of DNA
441 damage, computer-generated tail moment values (tail length × fraction of total DNA in the tail) were
442 used. A minimum of 200 cells was analysed for each experimental point. Apoptotic cells (smaller
443 comet head and extremely larger comet tail) were excluded from the analysis to avoid artificial
444 enhancement of the tail moment.
445
446 **Immunofluorescence**
447 Immunostaining for RNA-DNA hybrids was performed as described (Marabitti et al. 2019) . Briefly,
448 cells were fixed in 100% methanol for 10 min at -20°C, washed three times in PBS, pre-treated with
449 6 µg/ml of RNase A for 45 min at 37°C in 10 mM Tris-HCl pH 7.5 supplemented with 0.5 M NaCl,
450 before blocking in 2% BSA/PBS overnight at 4°C. Cells were then incubated with the anti-DNA-
451 RNA hybrid [S9.6] antibody (Kerafast, 1:100) overnight at 4°C. After each primary antibody, cells
452 were washed twice with PBS, and incubated with the specific secondary antibody: goat anti-mouse
453 Alexa Fluor-488 or goat anti-rabbit Alexa Fluor-594 (Molecular Probes). The incubation with
454 secondary antibodies were accomplished in a humidified chamber for 1 h at RT. DNA was
455 counterstained with 0.5 µg/ml DAPI.
456 Images were acquired randomly using Eclipse 80i Nikon Fluorescence Microscope, equipped with a
457 VideoConfocal (ViCo) system. For each time point, at least 200 nuclei were examined. Nuclear foci
458 were scored at a 40× magnification and only nuclei showing more than five bright foci were counted
459 as positive. Intensity per nucleus was calculated using ImageJ. Parallel samples incubated with either
460 the appropriate normal serum or only with the secondary antibody confirmed that the observed
461 fluorescence pattern was not attributable to artefacts.
462
463 **Dot blot analysis**
464 Dot blot analysis was performed according to the protocol reported elsewhere (Morales et al. 2016).
465 Genomic DNA was isolated by standard extraction with Phenol/Clorophorm/Isoamylic Alcohol (pH
466 8.0) followed by precipitation with 3 M NaOAc and 70% Ethanol. Isolated gDNA was randomly
467 fragmented overnight at 37°C with a cocktail of restriction enzymes (BsrgI, EcoRI, HindIII, XbaI)
468 supplemented with 1 M Spermidin. After incubation, digested DNA was cleaned up with
469 Phenol/Clorophorm extraction and standard Ethanol precipitation. After sample quantification, 5 µg
470 of digested DNA were incubated with RNaseH overnight at 37°C as a negative control. Five
471 micrograms of each sample were spotted onto a nitrocellulose membrane, blocked in 5% non-fat dry

472 milk and incubated with the anti-DNA-RNA hybrid [S9.6] antibody (Kerafast, 1:1000) overnight at
473 4°C. Horseradish peroxidase-conjugated goat specie-specific secondary antibody (Santa Cruz
474 Biotechnology, Inc.) was used. Quantification on scanned image of blot was performed using Image
475 Lab software.
476
477 **In situ PLA assay**
478 The in situ proximity-ligation assay (PLA; Sigma-Aldrich) was performed according to the
479 manufacturer's instructions. Exponential growing cells were seeded into 8-well chamber slides (Lab-
480 Tek, Sigma Aldrich) at a density of 1.5-2.5×10^4 cells/well. After the indicated treatment, cells were
481 permeabilized with 0.5% Triton X-100 for 10 min at 4°C, fixed with 3% formaldehyde/ 2% sucrose
482 solution for 10 min, and then blocked in 3% BSA/PBS for 15 min. After washing with PBS, cells
483 were incubated with the two relevant primary antibodies. For the detection of R-loops using PLA
484 with the anti-S9.6 antibody, cells were fixed with ice-cold methanol for 10 min and blocked in 2%
485 BSA/PBS for 1h at 37°C.
486 The primary antibodies used were: anti-FLAG (mouse-monoclonal; Sigma-Aldrich, 1:250), anti-
487 WRNIP1 (rabbit-polyclonal; Bethyl 1:500), anti-S9.6 (mouse-monoclonal; Kerafast, 1:100), anti-
488 PCNA (rabbit-polyclonal; Abcam 1:500), anti-RNA polII (mouse-monoclonal; Santa Cruz, 1:200),
489 recombinant anti-S9.6 (mouse-monoclonal; Kerafast, 1:100), anti-RAD51 (rabbit-polyclonal, Abcam
490 1:300) and anti-FANCD2 (mouse-monoclonal, Santacruz 1:100). The negative control consisted of
491 using only one primary antibody. Samples were incubated with secondary antibodies conjugated with
492 PLA probes MINUS and PLUS: the PLA Probe anti-Mouse PLUS and anti-Rabbit Minus (Sigma-
493 Aldrich). The incubation with all antibodies was accomplished in a humidified chamber for 1 h at
494 37°C. Next, the PLA probes MINUS and PLUS were ligated using their connecting oligonucleotides
495 to produce a template for rolling-cycle amplification. During amplification, the products were
496 hybridized with red fluorescence-labelled oligonucleotide. Samples were mounted in Prolong Gold
497 antifade reagent with DAPI (blue). Images were acquired randomly using Eclipse 80i Nikon
498 Fluorescence Microscope, equipped with a Video Confocal (ViCo) system.
499
500 **DNA fiber analysis**
501 Cells were pulse-labelled with 50 μM 5-chloro-2'-deoxyuridine (CldU) and 250 μM 5-iodo-2'-
502 deoxyuridine (IdU) at specified times, with or without treatment as reported in the experimental
503 schemes. DNA fibres were prepared and spread out as previously reported (Leuzzi et al. 2016) . For
504 immunodetection of labelled tracks the following primary antibodies were used: anti-CldU (rat-
505 monoclonal anti-BrdU/CldU; BU1/75 ICR1 Abcam, 1:100) and anti-IdU (mouse-monoclonal anti-

506 BrdU/IdU; clone b44 Becton Dickinson, 1:10). The secondary antibodies were goat anti-mouse Alexa
507 Fluor 488 or goat anti-rabbit Alexa Fluor 594 (Molecular Probes, 1:200). The incubation with
508 antibodies was accomplished in a humidified chamber for 1 h at RT.
509 Images were acquired randomly from fields with untangled fibres using Eclipse 80i Nikon
510 Fluorescence Microscope, equipped with a Video Confocal (ViCo) system. The length of green
511 labelled tracks was measured using the Image-J software, and values were converted into kilobases
512 using the conversion factor 1µm = 2.59 kb as reported (Basile et al. 2014). A minimum of 100
513 individual fibres were analysed for each experiment and the mean of at least three independent
514 experiments presented. Statistics were calculated using Graph Pad Prism Software.
515
516 **Statistical analysis**
517 Statistical analysis was performed using Prism 8 (GraphPad Software). Details of the individual
518 statistical tests are indicated in the figure legends and results. Statistical differences in all case were
519 determined by Student's t-test, Mann-Whitney test or Anova one way test. In all cases, not significant:
520 $P > 0.05$; * $P < 0.05$; ** $P < 0.01$; *** $P < 0.001$; **** $P < 0.0001$. All experiments were repeated at
521 least three times unless otherwise noted.
522
523 **ACKNOWLEDGEMENTS**

524 This research was funded by Associazione Italiana per la Ricerca sul Cancro to A.F. (IG #19971) and
525 to P.P. (IG #17383).

526 **REFERENCES**

527 Aguilera, Andrés, and Tatiana García-Muse. 2012. "R Loops: From Transcription Byproducts to
528 Threats to Genome Stability." *Molecular Cell* 46 (2): 115–24.
529 https://doi.org/10.1016/j.molcel.2012.04.009.

530 Allison, David F., and Gang Greg Wang. 2019. "R-Loops: Formation, Function, and Relevance to
531 Cell Stress." *Cell Stress* 3 (2): 38–46. https://doi.org/10.15698/cst2019.02.175.

532 Basile, Giorgia, Giuseppe Leuzzi, Pietro Pichierri, and Annapaola Franchitto. 2014. "Checkpoint-
533 Dependent and Independent Roles of the Werner Syndrome Protein in Preserving Genome
534 Integrity in Response to Mild Replication Stress." *Nucleic Acids Research* 42 (20): 12628–39.
535 https://doi.org/10.1093/nar/gku1022.

536 Belotserkovskii, Boris P., Silvia Tornaletti, Alicia D. D'Souza, and Philip C. Hanawalt. 2018. "R-
537 Loop Generation during Transcription: Formation, Processing and Cellular Outcomes." *DNA*
538 *Repair* 71: 69–81. https://doi.org/10.1016/j.dnarep.2018.08.009.

539 Bhatia, Vaibhav, Sonia I. Barroso, María L. García-Rubio, Emanuela Tumini, Emilia Herrera-
540 Moyano, and Andrés Aguilera. 2014. "BRCA2 Prevents R-Loop Accumulation and Associates
541 with TREX-2 MRNA Export Factor PCID2." *Nature* 511 (7509): 362–65.
542 https://doi.org/10.1038/nature13374.

543 Bish, Rebecca A., and Michael P. Myers. 2007. "Werner Helicase-Interacting Protein 1 Binds
544 Polyubiquitin via Its Zinc Finger Domain." *Journal of Biological Chemistry* 282 (32): 23184–
545 93. https://doi.org/10.1074/jbc.M701042200.

546 Boguslawski, Sophie J., Dennis E. Smith, Mary A. Michalak, Kenneth E. Mickelson, Clifford O.
547 Yehle, William L. Patterson, and Robert J. Carrico. 1986. "Characterization of Monoclonal
548 Antibody to DNA · RNA and Its Application to Immunodetection of Hybrids." *Journal of*
549 *Immunological Methods* 89 (1): 123–30. https://doi.org/10.1016/0022-1759(86)90040-2.

550 Boubakri, Hasna, Anne Langlois De Septenville, Enrique Viguera, and Bénédicte Michel. 2010. "The
551 Helicases DinG, Rep and UvrD Cooperate to Promote Replication across Transcription Units in
552 Vivo." *EMBO Journal* 29 (1): 145–57. https://doi.org/10.1038/emboj.2009.308.

553 Brambati, Alessandra, Luca Zardoni, Eleonora Nardini, Achille Pellicioli, and Giordano Liberi. 2020.
554 "The Dark Side of RNA:DNA Hybrids." *Mutation Research - Reviews in Mutation Research*
555 784: 108300. https://doi.org/10.1016/j.mrrev.2020.108300.

556 Cerritelli, Susana M., Ella G. Frolova, Chiguang Feng, Alexander Grinberg, Paul E. Love, and Robert
557 J. Crouch. 2003. "Failure to Produce Mitochondrial DNA Results in Embryonic Lethality in
558 Rnaseh1 Null Mice." *Molecular Cell* 11 (3): 807–15. https://doi.org/10.1016/S1097-
559 2765(03)00088-1.

560 Chang, Emily Yun-Chia, and Peter C Stirling. 2017. "Replication Fork Protection Factors Controlling
561 R-Loop Bypass and Suppression." *Genes* 8 (1). https://doi.org/10.3390/genes8010033.

562 Chang, Emily Yun Chia, Carolina A. Novoa, Maria J. Aristizabal, Yan Coulombe, Romulo Segovia,
563 Richa Chaturvedi, Yaoqing Shen, et al. 2017. "RECQ-like Helicases Sgs1 and BLM Regulate
564 R-Loop- Associated Genome Instabil." *Journal of Cell Biology* 216 (12): 3991–4005.
565 https://doi.org/10.1083/jcb.201703168.

566 Chappidi, Nagaraja, Zuzana Nascakova, Barbora Boleslavska, Ralph Zellweger, Esin Isik, Martin
567 Andrs, Shruti Menon, et al. 2020. "Fork Cleavage-Religation Cycle and Active Transcription
568 Mediate Replication Restart after Fork Stalling at Co-Transcriptional R-Loops." *Molecular Cell*
569 77 (3): 528-541.e8. https://doi.org/10.1016/j.molcel.2019.10.026.

570 Crosetto, Nicola, Marzena Bienko, Richard G. Hibbert, Tina Perica, Chiara Ambrogio, Tobias
571 Kensche, Kay Hofmann, Titia K. Sixma, and Ivan Dikic. 2008. "Human Wrnip1 Is Localized in
572 Replication Factories in a Ubiquitin-Binding Zinc Finger-Dependent Manner." *Journal of*
573 *Biological Chemistry* 283 (50): 35173–85. https://doi.org/10.1074/jbc.M803219200.

574 Crossley, Madzia P., Michael Bocek, and Karlene A. Cimprich. 2019. "R-Loops as Cellular
575 Regulators and Genomic Threats." *Molecular Cell* 73 (3): 398–411.
576 https://doi.org/10.1016/j.molcel.2019.01.024.

577 Gaillard, Hélène, and Andrés Aguilera. 2016. "Transcription as a Threat to Genome Integrity."
578 *Annual Review of Biochemistry* 85 (March): 291–317. https://doi.org/10.1146/annurev-
579 biochem-060815-014908.

580 Gan, Wenjian, Zhishuang Guan, Jie Liu, Ting Gui, Keng Shen, James L. Manley, and Xialu Li. 2011.
581 "R-Loop-Mediated Genomic Instability Is Caused by Impairment of Replication Fork
582 Progression." *Genes and Development* 25 (19): 2041–56. https://doi.org/10.1101/gad.17010011.

583 García-Muse, Tatiana, and Andrés Aguilera. 2016. "Transcription-Replication Conflicts: How They
584 Occur and How They Are Resolved." *Nature Reviews Molecular Cell Biology* 17 (9): 553–63.
585 https://doi.org/10.1038/nrm.2016.88.

García-Muse, Tatiana, and Andrés Aguilera. 2019. "R Loops: From Physiological to Pathological Roles." *Cell* 179 (3): 604–18. https://doi.org/10.1016/j.cell.2019.08.055.

García-Rubio, María L., Carmen Pérez-Calero, Sonia I. Barroso, Emanuela Tumini, Emilia Herrera-Moyano, Iván V. Rosado, and Andrés Aguilera. 2015. "The Fanconi Anemia Pathway Protects Genome Integrity from R-Loops." *PLoS Genetics* 11 (11): 1–17. https://doi.org/10.1371/journal.pgen.1005674.

Gómez-González, Belén, and Andrés Aguilera. 2019. "Transcription-Mediated Replication Hindrance: A Major Driver of Genome Instability." *Genes and Development* 33 (15–16): 1008–26. https://doi.org/10.1101/gad.324517.119.

Hamperl, Stephan, Michael J. Bocek, Joshua C. Saldivar, Tomek Swigut, and Karlene A. Cimprich. 2017. "Transcription-Replication Conflict Orientation Modulates R-Loop Levels and Activates Distinct DNA Damage Responses." *Cell* 170 (4): 774-786.e19. https://doi.org/10.1016/j.cell.2017.07.043.

Hatchi, Elodie, Konstantina Skourti-Stathaki, Steffen Ventz, Luca Pinello, Angela Yen, Kinga Kamieniarz-Gdula, Stoil Dimitrov, et al. 2015. "BRCA1 Recruitment to Transcriptional Pause Sites Is Required for R-Loop-Driven DNA Damage Repair." *Molecular Cell* 57 (4): 636–47. https://doi.org/10.1016/j.molcel.2015.01.011.

Helmrich, Anne, Monica Ballarino, and Laszlo Tora. 2011. "Collisions between Replication and Transcription Complexes Cause Common Fragile Site Instability at the Longest Human Genes." *Molecular Cell* 44 (6): 966–77. https://doi.org/10.1016/j.molcel.2011.10.013.

Huertas, Pablo, and Andrés Aguilera. 2003. "Cotranscriptionally Formed DNA:RNA Hybrids Mediate Transcription Elongation Impairment and Transcription-Associated Recombination." *Molecular Cell* 12 (3): 711–21. https://doi.org/10.1016/j.molcel.2003.08.010.

Kanu, N., T. Zhang, R. A. Burrell, A. Chakraborty, J. Cronshaw, C. Dacosta, E. Grönroos, et al. 2016. "RAD18, WRNIP1 and ATMIN Promote ATM Signalling in Response to Replication Stress." *Oncogene* 35 (30): 4009–19. https://doi.org/10.1038/onc.2015.427.

Kawabe, Yoh Ichi, Dana Branzei, Tomoko Hayashi, Hirobumi Suzuki, Takashi Masuko, Fumitoshi Onoda, Seok Jin Heo, et al. 2001. "A Novel Protein Interacts with the Werner's Syndrome Gene Product Physically and Functionally." *Journal of Biological Chemistry* 276 (23): 20364–69. https://doi.org/10.1074/jbc.C100035200.

616 Kawabe, Yoh ichi, Masayuki Seki, Akari Yoshimura, Katsuaki Nishino, Tomoko Hayashi, Takashi
617 Takeuchi, Sohta Iguchi, et al. 2006. "Analyses of the Interaction of WRNIP1 with Werner
618 Syndrome Protein (WRN) in Vitro and in the Cell." *DNA Repair* 5 (7): 816–28.
619 https://doi.org/10.1016/j.dnarep.2006.04.006.

620 Leuzzi, Giuseppe, Veronica Marabitti, Pietro Pichierri, and Annapaola Franchitto. 2016. " WRNIP 1
621 Protects Stalled Forks from Degradation and Promotes Fork Restart after Replication Stress ."
622 *The EMBO Journal* 35 (13): 1437–51. https://doi.org/10.15252/embj.201593265.

623 Li, Xialu, and James L. Manley. 2005. "Inactivation of the SR Protein Splicing Factor ASF/SF2
624 Results in Genomic Instability." *Cell* 122 (3): 365–78.
625 https://doi.org/10.1016/j.cell.2005.06.008.

626 Liang, Zhuobin, Fengshan Liang, Yaqun Teng, Xiaoyong Chen, Jingchun Liu, Simonne Longerich,
627 Timsi Rao, et al. 2019. "Binding of FANCI-FANCD2 Complex to RNA and R-Loops Stimulates
628 Robust FANCD2 Monoubiquitination." *Cell Reports* 26 (3): 564-572.e5.
629 https://doi.org/10.1016/j.celrep.2018.12.084.

630 Marabitti, Veronica, Giorgia Lillo, Eva Malacaria, Valentina Palermo, Pietro Pichierri, and
631 Annapaola Franchitto. 2020. "Checkpoint Defects Elicit a WRNIP1-Mediated Response to
632 Counteract R-Loop-Associated Genomic Instability." *Cancers* 12 (2).
633 https://doi.org/10.3390/cancers12020389.

634 Marabitti, Veronica, Giorgia Lillo, Eva Malacaria, Valentina Palermo, Massimo Sanchez, Pietro
635 Pichierri, and Annapaola Franchitto. 2019. "ATM Pathway Activation Limits R-Loop-
636 Associated Genomic Instability in Werner Syndrome Cells." *Nucleic Acids Research* 47 (7):
637 3485–3502. https://doi.org/10.1093/nar/gkz025.

638 Morales, Julio C., Patricia Richard, Praveen L. Patidar, Edward A. Motea, Tuyen T. Dang, James L.
639 Manley, and David A. Boothman. 2016. "XRN2 Links Transcription Termination to DNA
640 Damage and Replication Stress." *PLoS Genetics* 12 (7): 1–22.
641 https://doi.org/10.1371/journal.pgen.1006107.

642 Müller, Werner E., Gerhard Seibert, Rudolf Beyer, Hans J. Breter, Armin Maidhof, and Rudolf K.
643 Zahn. 1977. "Effect of Cordycepin on Nucleic Acid Metabolism in L5178Y Cells and on Nucleic
644 Acid-Synthesizing Enzyme Systems." *Cancer Research* 37 (10): 3824–33.

645 Murfuni, Ivana, Anita De Santis, Maurizio Federico, Margherita Bignami, Pietro Pichierri, and

646 Annapaola Franchitto. 2012. "Perturbed Replication Induced Genome Wide or at Common
647 Fragile Sites Is Differently Managed in the Absence of WRN." *Carcinogenesis* 33 (9): 1655–
648 63. https://doi.org/10.1093/carcin/bgs206.

649 Nomura, Hironoshin, Akari Yoshimura, Takato Edo, Shin Ichiro Kanno, Syusuke Tada, Masayuki
650 Seki, Akira Yasui, and Takemi Enomoto. 2012. "WRNIP1 Accumulates at Laser Light
651 Irradiated Sites Rapidly via Its Ubiquitin-Binding Zinc Finger Domain and Independently from
652 Its ATPase Domain." *Biochemical and Biophysical Research Communications* 417 (4): 1145–
653 50. https://doi.org/10.1016/j.bbrc.2011.12.080.

654 Paulsen, Renee D., Deena V. Soni, Roy Wollman, Angela T. Hahn, Muh Ching Yee, Anna Guan,
655 Jayne A. Hesley, et al. 2009. "A Genome-Wide SiRNA Screen Reveals Diverse Cellular
656 Processes and Pathways That Mediate Genome Stability." *Molecular Cell* 35 (2): 228–39.
657 https://doi.org/10.1016/j.molcel.2009.06.021.

658 Pichierri, Pietro, Annapaola Franchitto, Pasquale Mosesso, Fabrizio Palitti. 2001. "Werner ' s
659 Syndrome Protein Is Required for Correct Recovery after Replication Arrest and DNA Damage
660 Induced in S-Phase of Cell Cycle." *Molecular Biology of the Cell* 12 (August): 2412–21.

661 Pirzio, Livia Maria, Pietro Pichierri, Margherita Bignami, and Annapaola Franchitto. 2008. "Werner
662 Syndrome Helicase Activity Is Essential in Maintaining Fragile Site Stability." *The Journal of*
663 *Cell Biology* 180 (2): 305–14. https://doi.org/10.1083/jcb.200705126.

664 Pladevall-Morera, David, Stephanie Munk, Andreas Ingham, Lorenza Garribba, Eliene Albers, Ying
665 Liu, Jesper V. Olsen, and Andres J. Lopez-Contreras. 2019. "Proteomic Characterization of
666 Chromosomal Common Fragile Site (CFS)-Associated Proteins Uncovers ATRX as a Regulator
667 of CFS Stability." *Nucleic Acids Research* 47 (15): 8004–18.
668 https://doi.org/10.1093/nar/gkz510.

669 Porebski, Bartlomiej, Sebastian Wild, Sandra Kummer, Sarah Scaglione, Pierre Henri L. Gaillard,
670 and Kerstin Gari. 2019. "WRNIP1 Protects Reversed DNA Replication Forks from SLX4-
671 Dependent Nucleolytic Cleavage." *IScience* 21: 31–41.
672 https://doi.org/10.1016/j.isci.2019.10.010.

673 Promonet, Alexy, Ismaël Padioleau, Yaqun Liu, Lionel Sanz, Anna Biernacka, Anne Lyne Schmitz,
674 Magdalena Skrzypczak, et al. 2020. "Topoisomerase 1 Prevents Replication Stress at R-Loop-
675 Enriched Transcription Termination Sites." *Nature Communications* 11 (1): 1–12.
676 https://doi.org/10.1038/s41467-020-17858-2.

677 Santos-Pereira, José M., and Andrés Aguilera. 2015. "R Loops: New Modulators of Genome
678 Dynamics and Function." *Nature Reviews Genetics* 16 (10): 583–97.
679 https://doi.org/10.1038/nrg3961.

680 Sanz, Lionel A., Stella R. Hartono, Yoong Wearn Lim, Sandra Steyaert, Aparna Rajpurkar, Paul A.
681 Ginno, Xiaoqin Xu, and Frédéric Chédin. 2016. "Prevalent, Dynamic, and Conserved R-Loop
682 Structures Associate with Specific Epigenomic Signatures in Mammals." *Molecular Cell* 63 (1):
683 167–78. https://doi.org/10.1016/j.molcel.2016.05.032.

684 Schwab, Rebekka A., Jadwiga Nieminuszczy, Fenil Shah, Jamie Langton, David Lopez Martinez,
685 Chih Chao Liang, Martin A. Cohn, Richard J. Gibbons, Andrew J. Deans, and Wojciech
686 Niedzwiedz. 2015. "The Fanconi Anemia Pathway Maintains Genome Stability by Coordinating
687 Replication and Transcription." *Molecular Cell* 60 (3): 351–61.
688 https://doi.org/10.1016/j.molcel.2015.09.012.

689 Shivji, Mahmud K.K., Xavier Renaudin, Çiğdem H. Williams, and Ashok R. Venkitaraman. 2018.
690 "BRCA2 Regulates Transcription Elongation by RNA Polymerase II to Prevent R-Loop
691 Accumulation." *Cell Reports* 22 (4): 1031–39. https://doi.org/10.1016/j.celrep.2017.12.086.

692 Socha, Anna, Di Yang, Alicja Bulsiewicz, Kelvin Yaprianto, Marian Kupculak, Chih Chao Liang,
693 Andreas Hadjicharalambous, Ronghu Wu, Steven P. Gygi, and Martin A. Cohn. 2020.
694 "WRNIP1 Is Recruited to DNA Interstrand Crosslinks and Promotes Repair." *Cell Reports* 32
695 (1): 107850. https://doi.org/10.1016/j.celrep.2020.107850.

696 Söderberg, Ola, Karl Johan Leuchowius, Mats Gullberg, Malin Jarvius, Irene Weibrecht, Lars Gunnar
697 Larsson, and Ulf Landegren. 2008. "Characterizing Proteins and Their Interactions in Cells and
698 Tissues Using the in Situ Proximity Ligation Assay." *Methods* 45 (3): 227–32.
699 https://doi.org/10.1016/j.ymeth.2008.06.014.

700 Sollier, Julie, Caroline Townsend Stork, María L. García-Rubio, Renee D. Paulsen, Andrés Aguilera,
701 and Karlene A. Cimprich. 2014. "Transcription-Coupled Nucleotide Excision Repair Factors
702 Promote R-Loop-Induced Genome Instability." *Molecular Cell* 56 (6): 777–85.
703 https://doi.org/10.1016/j.molcel.2014.10.020.

704 Stoy, Henriette, Katharina Zwicky, Danina Kuster, Kevin S Lang, Jana Krietsch, Magdalena P
705 Crossley, Jonas A Schmid, Karlene A Cimprich, Houra Merrikh, and Massimo Lopes. 2023.
706 "Direct Visualization of Transcription-Replication Conflicts Reveals Post-Replicative
707 DNA:RNA Hybrids." *Nature Structural & Molecular Biology* 30 (3): 348–59.

https://doi.org/10.1038/s41594-023-00928-6.

Taniguchi, Toshiyasu, Irene Garcia-Higuera, Paul R Andreassen, Richard C Gregory, Markus Grompe, and Alan D D'Andrea. 2002. "S-Phase-Specific Interaction of the Fanconi Anemia Protein, FANCD2, with BRCA1 and RAD51." *Blood* 100 (7): 2414–20. https://doi.org/10.1182/blood-2002-01-0278.

Tresini, Maria, Daniël O. Warmerdam, Petros Kolovos, Loes Snijder, Mischa G. Vrouwe, Jeroen A.A. Demmers, Wilfred F.J. Van Ijcken, et al. 2015. "The Core Spliceosome as Target and Effector of Non-Canonical ATM Signalling." *Nature* 523 (7558): 53–58. https://doi.org/10.1038/nature14512.

Tuduri, Sandie, Laure Crabbé, Chiara Conti, Hélène Tourrière, Heidi Holtgreve-Grez, Anna Jauch, Véronique Pantesco, et al. 2009. "Topoisomerase I Suppresses Genomic Instability by Preventing Interference between Replication and Transcription." *Nature Cell Biology* 11 (11): 1315–24. https://doi.org/10.1038/ncb1984.

Urban, Vaclav, Jana Dobrovolna, Daniela Hühn, Jana Fryzelkova, Jiri Bartek, and Pavel Janscak. 2016. "RECQ5 Helicase Promotes Resolution of Conflicts between Replication and Transcription in Human Cells." *Journal of Cell Biology* 214 (4): 401–15. https://doi.org/10.1083/jcb.201507099.

Wahba, Lamia, Jeremy D. Amon, Douglas Koshland, and Milena Vuica-Ross. 2011. "RNase H and Multiple RNA Biogenesis Factors Cooperate to Prevent RNA:DNA Hybrids from Generating Genome Instability." *Molecular Cell* 44 (6): 978–88. https://doi.org/10.1016/j.molcel.2011.10.017.

Wang, Yan, Binbin Ma, Xiaoxu Liu, Ge Gao, Zhuanzhuan Che, Menghan Fan, Siyan Meng, et al. 2022. "ZFP281-BRCA2 Prevents R-Loop Accumulation during DNA Replication." *Nature Communications* 13 (1): 3493. https://doi.org/10.1038/s41467-022-31211-9.

Ward, Irene M., and Junjie Chen. 2001. "Histone H2AX Is Phosphorylated in an ATR-Dependent Manner in Response to Replicational Stress." *Journal of Biological Chemistry* 276 (51): 47759–62. https://doi.org/10.1074/jbc.C100569200.

Wellinger, Ralf E., Félix Prado, and Andrés Aguilera. 2006. "Replication Fork Progression Is Impaired by Transcription in Hyperrecombinant Yeast Cells Lacking a Functional THO Complex." *Molecular and Cellular Biology* 26 (8): 3327–34.

https://doi.org/10.1128/mcb.26.8.3327-3334.2006.

Wells, James P, Emily Yun-Chia Chang, Leticia Dinatto, Justin White, Stephanie Ryall, and Peter C Stirling. 2022. "RAD18 Opposes Transcription-Associated Genome Instability through FANCD2 Recruitment." *PLoS Genetics* 18 (12): e1010309. https://doi.org/10.1371/journal.pgen.1010309.

Yoshimura, Akari, Masayuki Seki, and Takemi Enomoto. 2017. "The Role of WRNIP1 in Genome Maintenance." *Cell Cycle* 16 (6): 515–21. https://doi.org/10.1080/15384101.2017.1282585.

Yoshimura, Akari, Masayuki Seki, Makoto Kanamori, Satoshi Tateishi, Toshiki Tsurimoto, Shusuke Tada, and Takemi Enomoto. 2009. "Physical and Functional Interaction between WRNIP1 and RAD18." *Genes and Genetic Systems* 84 (2): 171–78. https://doi.org/10.1266/ggs.84.171.

750 **FIGURES**

751

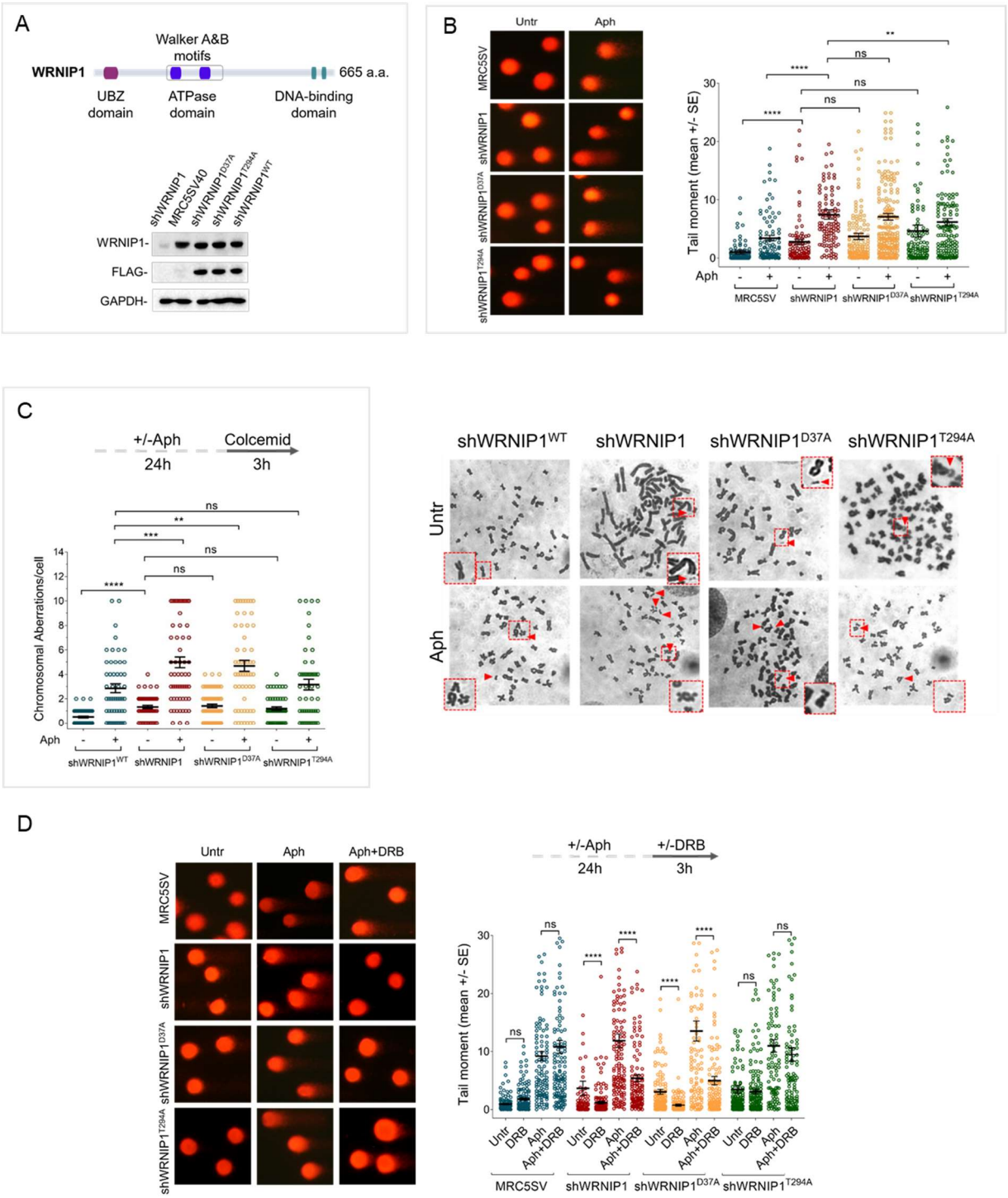

752 **Figure 1. Loss of WRNIP1 or its UBZ domain results in DNA damage accumulation and**
753 **enhanced chromosomal instability upon MRS**

754 (A) Schematic representation of human WRNIP1 protein structure. Western blot analysis showing
755 the expression of the WRNIP1 protein in wild-type cells (shWRNIP1^{WT}), WRNIP1-deficient cells
756 (shWRNIP1) and WRNIP1 ATPase mutant (shWRNIP1^{T294A}) or WRNIP1 UBZ mutant

757 (shWRNIP1^{D37A}) cells. MRC5SV40 fibroblasts were used as a positive control. The membrane was
758 probed with an anti-FLAG or anti-WRNIP1 antibody. GAPDH was used as a loading control.
759 (B) Analysis of DNA damage accumulation evaluated by alkaline Comet assay. MRC5SV,
760 shWRNIP1, shWRNIP1^{D37A} and shWRNIP1^{T294A} cells were treated or not with 0.4 μM Aph for 24
761 h, then subjected to Comet assay. The graph shows data presented as mean tail moment ± SE from
762 three independent experiments. Horizontal black lines represent the mean (ns, not significant; **, P
763 < 0.01; ****, $P < 0.0001$; two-tailed Student's t test). Representative images are given.
764 (C) Analysis of chromosomal aberrations in the indicated cell lines treated as shown in the
765 experimental scheme. Dot plot shows the number of chromosomal aberrations per cell ± SE from
766 three independent experiments. Horizontal black lines represent the mean (ns, not significant; **, P
767 < 0.01; ***, $P < 0.001$; ****, $P < 0.0001$; two-tailed Student's t test). Representative images are
768 given. Insets show enlarged metaphases for a better visualization of chromosomal aberrations.
769 (D) Evaluation of DNA damage accumulation by alkaline Comet assay. Cells were treated as shown
770 in the experimental scheme, then subjected to Comet assay. Dot plot shows data presented as mean
771 tail moment ± SE from three independent experiments. Horizontal black lines represent the mean (ns,
772 not significant; ****, $P < 0.0001$; two-tailed Student's t test). Representative images are given.
773

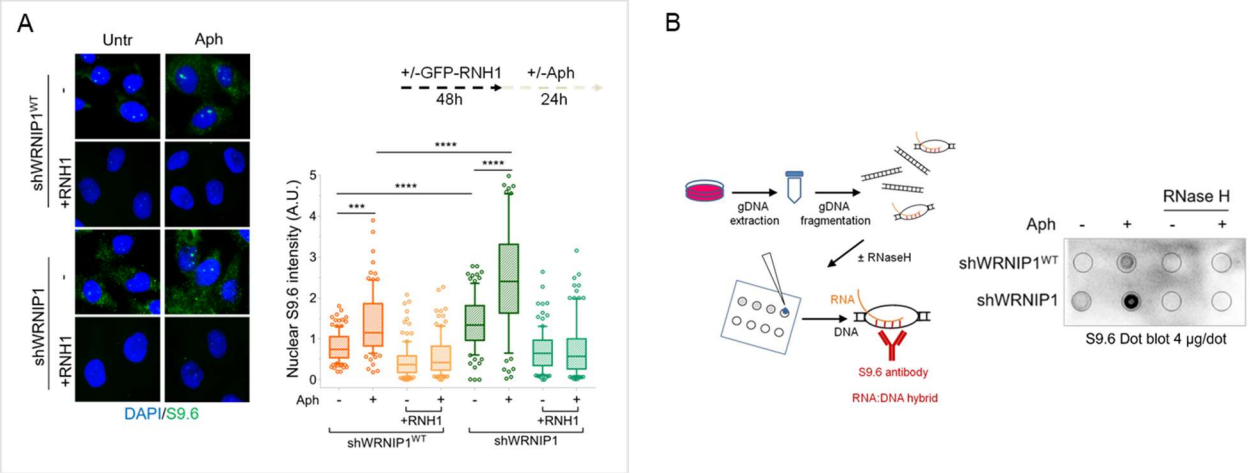

Figure 2. **Loss of WRNIP1 or its UBZ domain results in R-loop accumulation upon MRS**

(**A**) Evaluation of R-loop accumulation by immunofluorescence analysis in shWRNIP1^{WT} and shWRNIP1 cells treated as reported in the experimental design after transfection with GFP-tagged RNaseH1 or empty vector. Cells were fixed and stained with anti-RNA-DNA hybrid S9.6 monoclonal antibody. Representative images are given. Nuclei were counterstained with DAPI. Box plot shows nuclear S9.6 fluorescence intensity. Box and whiskers represent 20-75 and 10-90 percentiles, respectively. The line represents the median value. Data are presented as means of three independent experiments. Horizontal black lines represent the mean. Error bars represent standard error (***, $P < 0.001$; ****, $P < 0.0001$; two-tailed Student's t test).

(**B**) Dot blot to confirm R-loop accumulation. Genomic DNA isolated from shWRNIP1WT and shWRNIP1 cells, treated as reported in the experimental design and processed as described in "Materials and Methods", was spotted onto nitrocellulose membrane. The membrane was probed with anti-RNA-DNA hybrid S9.6 monoclonal antibody. Treatment with RNase H was used as a negative control. Representative gel images of at least three replicates are shown.

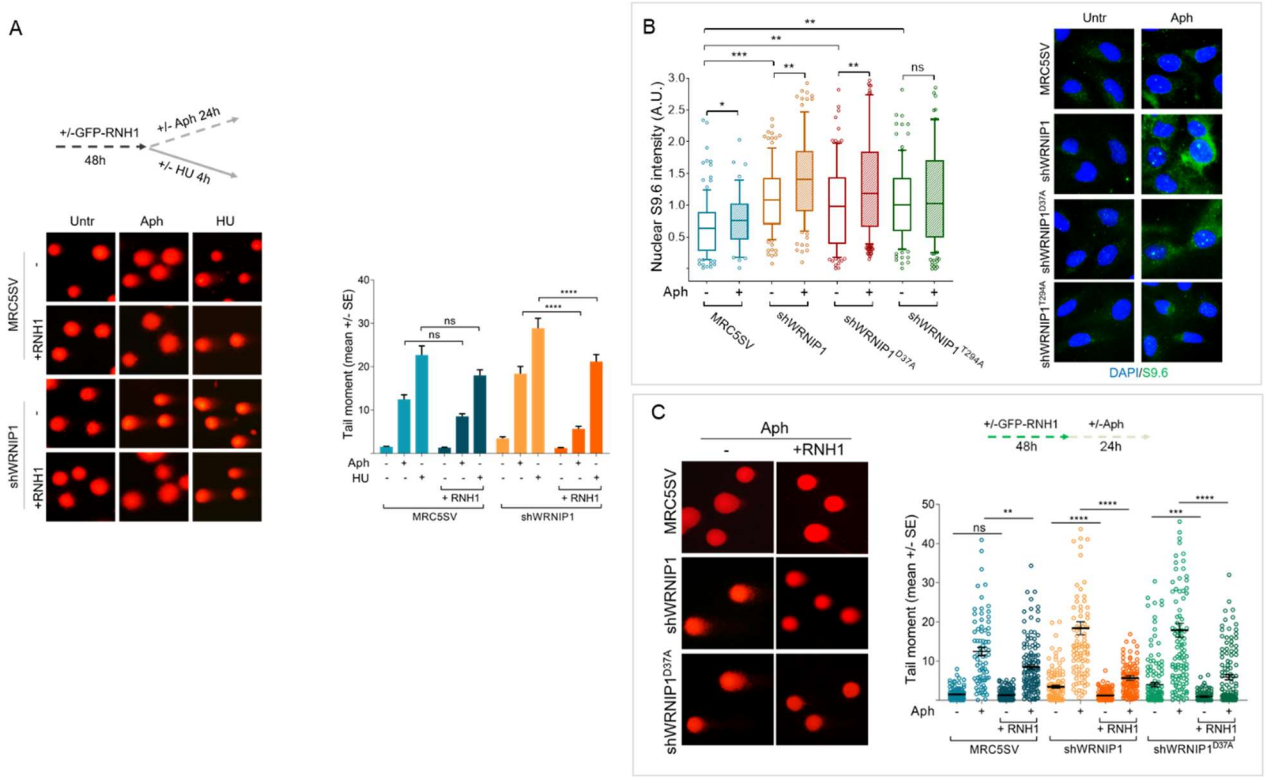

Figure 3. **Loss of WRNIP1 or its UBZ domain leads to R-loop-dependent accumulation upon MRS**

(**A**) Analysis of DNA damage accumulation by alkaline Comet assay. MRC5SV and shWRNIP1 cells were treated or not with Aph or HU, as reported by the experimental scheme after transfection with GFP-tagged RNaseH1 or empty vector (-),then subjected to Comet assay. The graph shows data presented as mean tail moment ± SE from three independent experiments (ns, not significant; **** $P < 0.0001$; two-tailed Student's t test). Representative images are given.

(**B**) Immunofluorescence analysis to determine R-loop levels in MRC5SV, shWRNIP1, shWRNIP1^{D37A} and shWRNIP1^{T294A} cells treated or not with 0.4 μM Aph for 24 h. Cells were fixed and stained with anti-RNA-DNA hybrid S9.6 monoclonal antibody. Representative images are given. Nuclei were counterstained with DAPI. Box plot shows nuclear S9.6 fluorescence intensity. Box and whiskers represent 20-75 and 10-90 percentiles, respectively. The line represents the median value. Data are presented as means of three independent experiments. Horizontal black lines represent the mean. Error bars represent SE (ns, not significant; * $P < 0.05$; ** $P < 0.01$; ***, $P < 0.001$; two-tailed Student's t test).

807 (**C**) Analysis of the effect of R-loop resolution on DNA damage accumulation evaluated by alkaline
808 Comet assay. Cells were treated as reported in the experimental scheme after transfection with GFP-
809 tagged RNaseH1 or empty vector, then subjected to Comet assay. Dot plot shows data presented as
810 mean tail moment ± SE from three independent experiments. Horizontal black lines represent the
811 mean (ns, not significant; ** $P < 0.01$; *** $P < 0.001$; **** $P < 0.0001$; two-tailed Student's t test).
812 Representative images are given.
813

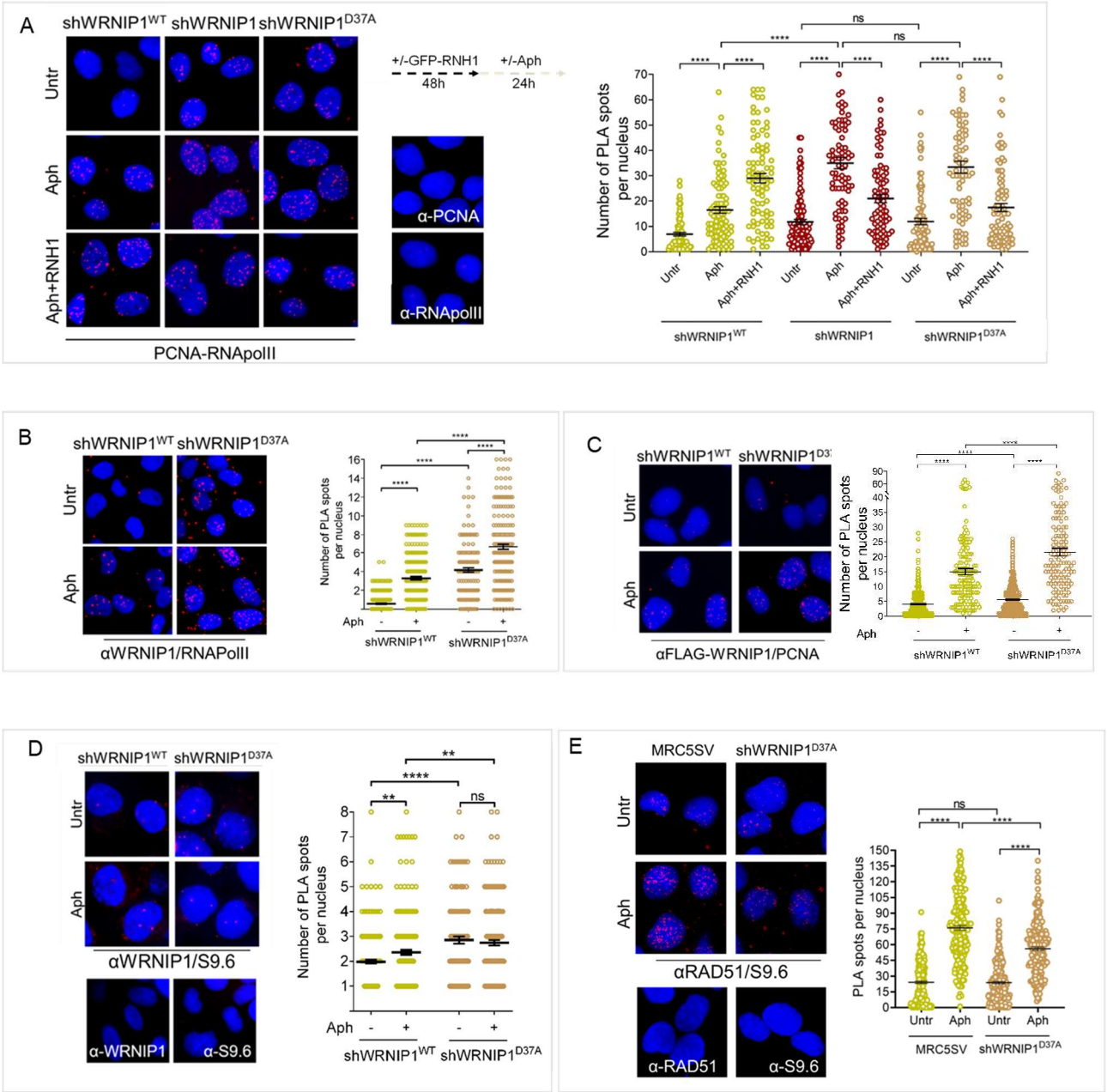

Figure 4. Loss of WRNIP1 or its UBZ domain promotes R-loop-dependent TRCs accumulation (**A**) Detection of TRCs by fluorescence-based PLA assay in MRC5SV, shWRNIP1 and shWRNIP1^{D37A} cells treated as reported in the experimental scheme after transfection with GFP-tagged RNaseH1 or empty vector. Cells were fixed and stained with antibodies against PCNA and RNA pol II. Representative images are given. Each red spot represents a single interaction between proteins. No spot has been revealed in cells stained with each single antibody (negative control). Nuclei were counterstained with DAPI. Dot plot shows the number of PLA spots per nucleus. Data are presented as means of three independent experiments. Horizontal black lines represent the mean ± SE (ns, not significant; ****, $P < 0.0001$; Mann-Whitney test).

824 (**B** and **C**) Analysis of localization of WRNIP1 near/at the transcription and replication machineries
825 by PLA. Cells were treated or not with 0.4 μM Aph for 24 h, fixed and stained with antibodies against
826 WRNIP1 and RNA pol II (**B**) or WRNIP1 and PCNA (**C**) to visualize the interaction between
827 WRNIP1 and replication or transcription machinery, respectively. Each red spot represents a single
828 interaction between proteins. Representative images are given. Nuclei were counterstained with
829 DAPI. Dot plots show the number of PLA spots per nucleus. Data are presented as means of three
830 independent experiments. Horizontal black lines represent the mean ± SE (****, $P < 0.0001$; Anova
831 one-way test).
832 (**D** and **E**) Detection of physical interaction between WRNIP1 and R-loops (**D**) or R-loops and
833 RAD51(**E**). Cells were treated or not with 0.4 μM Aph for 24 h, followed by the PLA assay described
834 in "Supplementary Materials and Methods". Cells were stained with antibodies against RNA-DNA
835 hybrid (anti-S9.6) and WRNIP1 (**D**) or RNA-DNA hybrid (anti-S9.6) and RAD51 (**E**).
836 Representative images are given. Each red spot represents a single interaction between R-loops and
837 the respective proteins (WRNIP1 or RAD51). No spot has been revealed in cells stained with each
838 single antibody (negative control). Nuclei were counterstained with DAPI. Dot plot shows the number
839 of PLA spots per nucleus. Horizontal black lines represent the mean ± SE (ns, not significant; ** $P <$
840 0.01****, $P < 0.0001$; Anova one-way test).
841

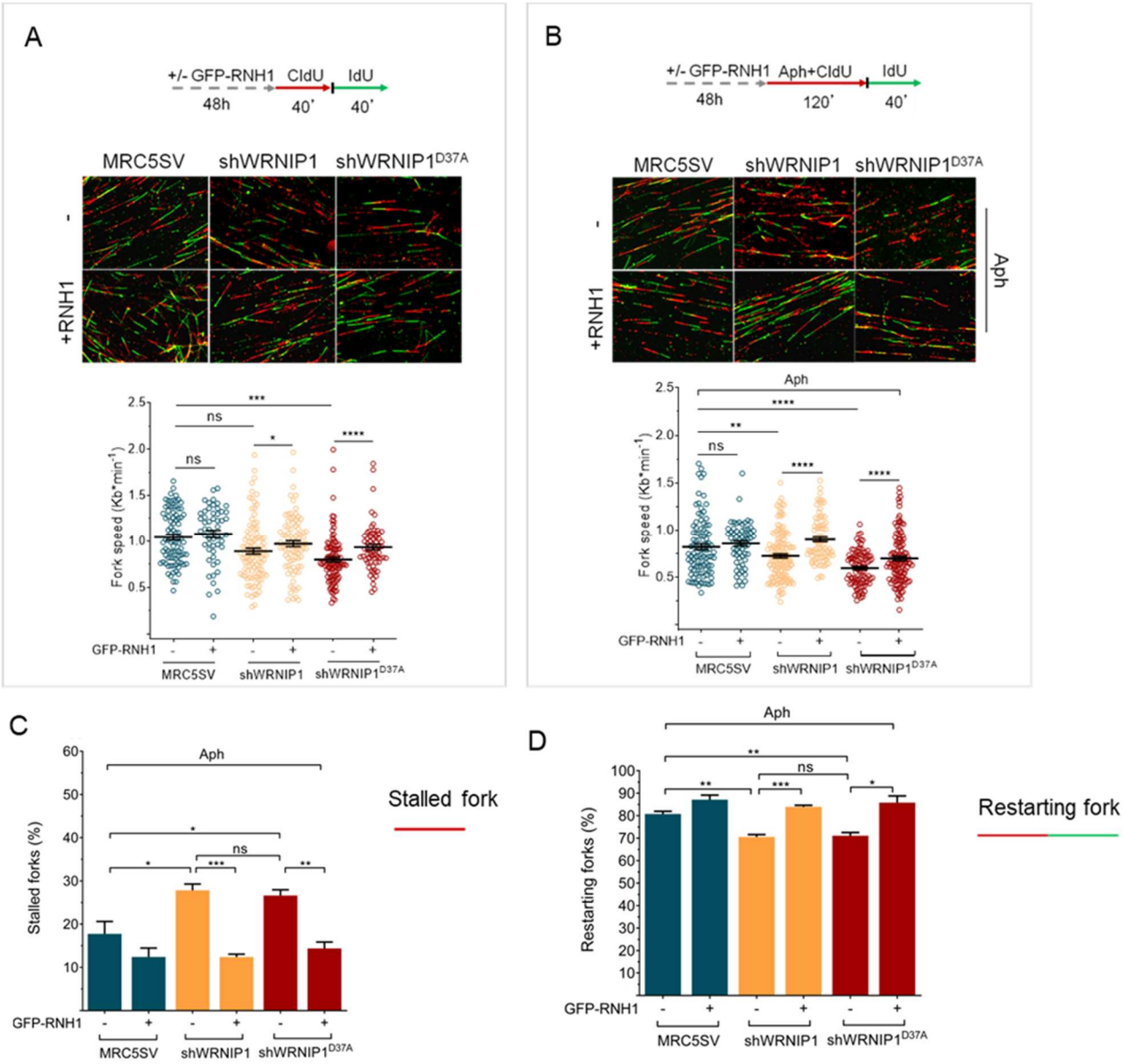

Figure 5. R-loops affects DNA replication in cells lacking WRNIP1 or its UBZ domain upon MRS

Experimental scheme of dual labelling of DNA fibers in MRC5SV, shWRNIP1 and shWRNIP1^{D37A} cells under unperturbed conditions (**A**) or upon MRS (**B**). After transfection with GFP-tagged RNaseH1 or empty vector (-), cells were pulse-labelled with CldU, treated or not with 0.4 µM Aph, then subjected to a pulse-labelling with IdU. Representative DNA fiber images are shown. The graph shows the analysis of replication fork velocity (fork speed) in the cells. The length of the green tracks was measured. Mean values are represented as horizontal black lines (ns, not significant; *, $P < 0.05$; **, $P < 0.01$; ***, $P < 0.001$; ****, $P < 0.0001$; Mann-Whitney test). (**C** and **D**) The graph shows the percentage of red (CldU) tracts (stalled forks) or green (IdU) tracts (restarting forks) in the cells. Error bars represent standard error (ns, not significant; *, $P < 0.05$; ** $P < 0.01$; *** $P < 0.001$; two tailed Student t-test).

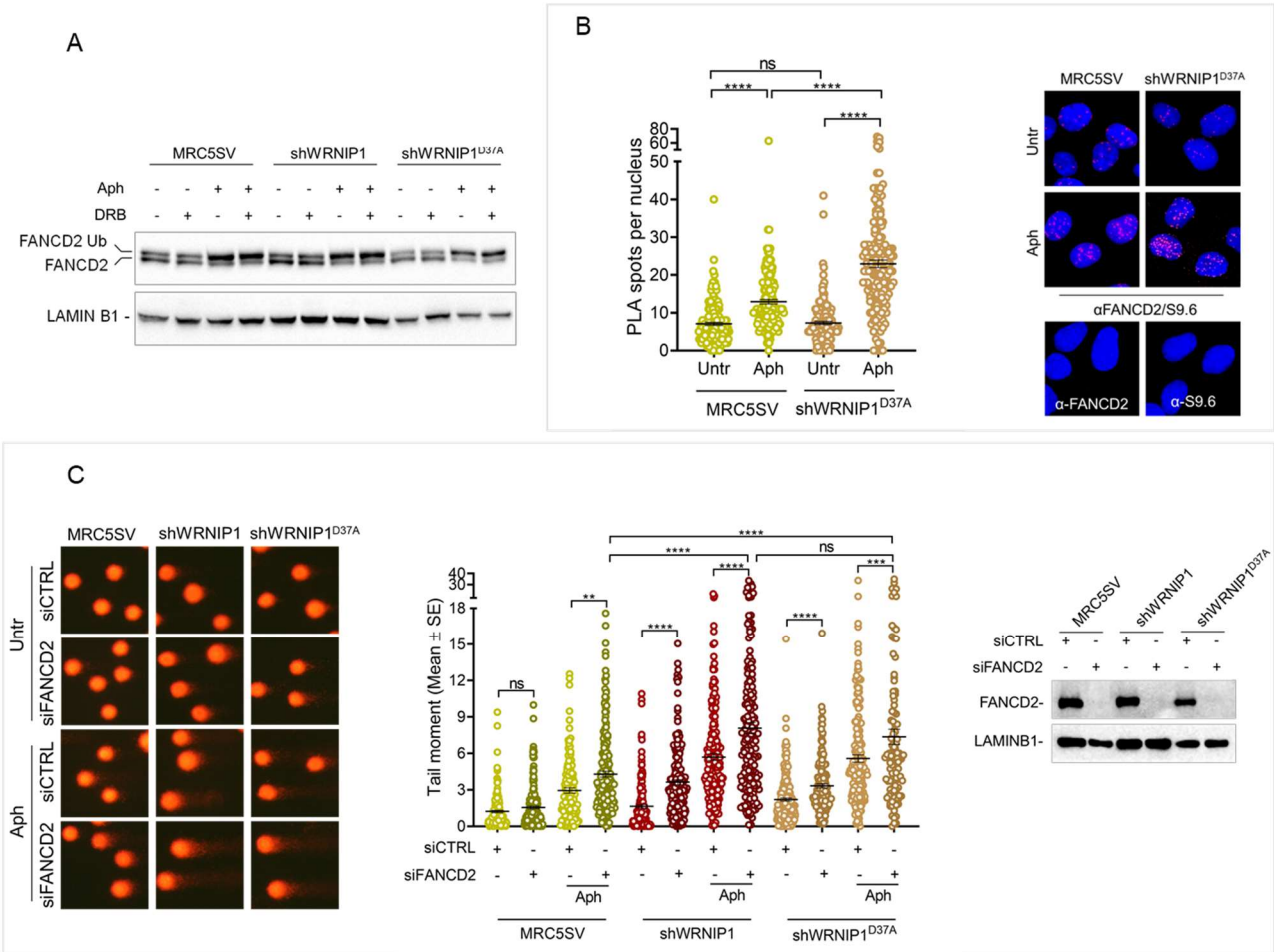

855

856 **Figure 6. FANCD2 pathway activation in cells lacking WRNIP1 or its UBZ domain upon MRS**

857 (**A**) Western blot analysis showing FANCD2 ubiquitination in MRC5SV, shWRNIP1 and
858 shWRNIP1^{D37A} cells. The membrane was probed with an anti-FANCD2 antibody. LAMIN B1 was
859 used as a loading control.

860 (**B**) Detection of physical interaction between FANCD2 and R-loops by PLA. MRC5SV and
861 shWRNIP1^{D37A} cells treated with or not with 0.4 µM Aph for 24h. Cells were stained with antibodies
862 against RNA-DNA hybrid (anti-S9.6) and FANCD2. Representative images are given. Each red spot
863 represents a single interaction between R-loops and FANCD2. No spot has been revealed in cells
864 stained with each single antibody (negative control). Nuclei were counterstained with DAPI. Dot plot
865 shows the number of PLA spots per nucleus. Data are presented as means of three independent
866 experiments. Horizontal black lines represent the mean ± SE (ns, not significant; ****, $P < 0.0001$;
867 Anova one-way test).

868 (**C**) Evaluation of DNA damage accumulation by alkaline comet assay in MRC5SV, shWRNIP1 and
869 shWRNIP1^{D37A} transfected with control siRNAs (siCTRL) or siRNAs targeting FANCD2
870 (siFANCD2). After 48 h, cells were treated with 0.4 µM Aph for 24h, then subjected to Comet assay.
871 Dot plot shows data presented as the mean tail moment ± SE from three independent experiments.

872 Horizontal black lines represent the mean (ns, not significant; ** $P < 0.01$; *** $P < 0.001$; **** $P <$
873 0.0001; two-tailed Student's t test). Representative images are given. Western blot shows FANCD2
874 depletion in the cells. The membrane was probed with an anti-FANCD2 and LAMIN B1 was used as
875 a loading control.